Coordination polymers of various architectures built with mixed imidazole/benzimidazole and carboxylate donor ligands and different metal ions: syntheses, structural features and magnetic properties†‡

Arshad Aijaz,[a] Prem Lama,[a] E. Carolina Sañudo,[b] Rupali Mishra[a] and Parimal K. Bharadwaj*[a]

Received (in Victoria, Australia) 20th April 2010, Accepted 8th August 2010
DOI: 10.1039/c0nj00302f

Ten coordination polymers $\{[Cd(L_1)_2]\}_n$ (**1**), $\{[Cu(L_1)_2]\}_n$ (**2**), $\{[Cd_2(L_1)_2(HCOO)_2(H_2O)]\}_n$ (**3**), $\{[Cd_2(L_1)_4]\cdot 3H_2O\}_n$ (**4**), $\{[Cd(L_1)(CH_3COO)]\}_n$ (**5**), $\{[Cd(L_1)_2(C_5H_5N)]\cdot 2.5H_2O\}_n$ (**6**), $\{[Zn(L_2)_2]\}_n$ (**7**), $\{[Cd_2(L_2)_4]\cdot H_2O\}_n$ (**8**), $\{[Cd_3(L_2)_6(H_2O)]\cdot 2EtOH\cdot H_2O\}_n$ (**9**) and $\{[Cd(L_3)_2]\cdot 2DMF\cdot 4H_2O\}_n$ (**10**), where HL_1 = 4-imidazole-1-yl-benzoic acid, HL_2 = 3-imidazole-1-yl-benzoic acid and HL_3 = 4-benzmidazole-1-yl-benzoic acid, have been synthesized under different experimental conditions. Their structures are determined by single-crystal X-ray diffraction analyses and further characterized by IR spectra, thermogravimetric (TG) and elemental analyses. The structure of **1** is a 2D → 2D (2D = two dimensional) interpenetrating network with (4,4) grid topology while **2** has an interesting Kagome structure. Compounds **4** and **6** crystallize in 4- and 3-fold interpenetrating diamondoid frameworks respectively. Compound **7** is a layered non-interpenetrating (4,4) grid network whereas **8** has an unprecedented self-penetrating structure with 2D framework. Compound **9** is a self-penetrating 3D structure while **10** crystallizes in a non-interpenetrating (4,4) square-grid with one-dimensional (1D) channels. From these results, it is demonstrated that the structures of the coordination polymers are strongly dependent on the geometry of $\mathbf{L_1}$, $\mathbf{L_2}$ and reaction conditions. Variable temperature magnetic susceptibility study of **2** has also been performed.

Introduction

The rational design of new coordination polymers is of enormous current interest because of their potential applications in several contemporary problems.[1–5] During the past decade, judicious combination of organic ligands as "spacers" and metal ions as "nodes" have been the common synthetic approach to produce coordination polymers.[6] In particular, a large number of noteworthy 2D and 3D frameworks containing cavities with diverse sizes and shapes have been engineered by the assembly of ditopic ligands and square planar or octahedral metal centers.[7] So far, the synthetic focus in this area of research has been centered on the exploitation of the rod-like and symmetrically bridging ligands.[8] Use of unsymmetrical ligands, possessing two or more coordination sites with different donor ability, can be assembled around metal centers in diverse arrangements, resulting in structures with novel topological features.[9] The development and identification of novel solid-state architectures is a general theme in the pursuit of new functional materials. However, at times, finding strategies to prepare a designed solid-state architecture can be highly empirical, and obtaining a phase with the desired organization of components becomes a trial and error process. Coordination polymer structures can be synthesized by hydro-(solvo)thermal or room temperature reactions between metal ions and multi-dentate ligands. In most cases, it may not be possible to predict the structural pattern by looking at the ligand structure while, in a few cases, unexpected reactions[10] such as ligand oxidative coupling, hydrolysis or substitution, can occur making it almost impossible to predict the final structure. However, such ligand transformations provide alternate routes for the construction of new coordination polymers.

It has been noted that coordination complexes with *in situ* generated ligands are of great interest both in coordination chemistry and organic chemistry for discovery of new organic reactions and understanding the reaction mechanisms, as well as for preparation of network architectures that are usually inaccessible *via* direct use of the ligands.[11] However, there is presently very little understanding concerning the factors that determine their synthesis and the attainment of rational control over desired topologies. In fact, we were unable to generate some of the polymers like (4,4) net with similar type of ligands under same or different conditions *via* direct use of the ligand, but those were obtained by *in situ* cyanide hydrolysis.

Herein, we have chosen ligands with imidazole/benzimidazole and carboxylate donors at the terminals (Scheme 1). These ligands are an extension of our previously reported ligand.[12] The ligands are chosen because they have (1) rotatable single

[a] *Chemistry Department, Indian Institute of Technology, Kanpur, 208016, India. E-mail: pkb@iitk.ac.in; Fax: (+91)-512-2597436; Tel: (+91)-512-2597304*
[b] *Departament de Química Inorgànica, Universitat de Barcelona, Diagonal, 647, 08028-Barcelona, Spain*

† This article is part of a themed issue on Coordination polymers: structure and function.

‡ Electronic supplementary information (ESI) available: Additional figures and selected bond distances and bond angles. CCDC reference numbers 773576–773585. For ESI and crystallographic data in CIF or other electronic format see DOI: 10.1039/c0nj00302f

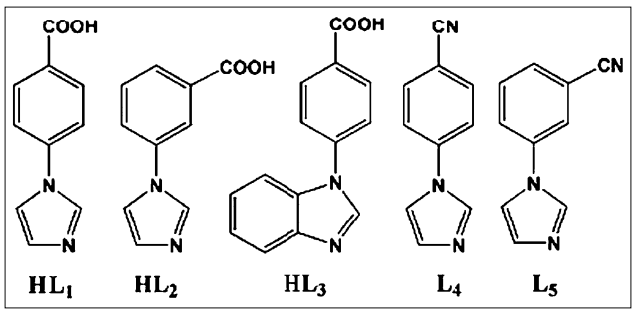

Scheme 1 Ligands used for the construction of coordination polymers.

C–N bond(s) that impart a variety of topological structures, (2) rigid rod-like nature that is potentially attractive for having porous structures and (3) carboxylate groups that help to create neutral frameworks without anions in the pores. We have synthesized a series of coordination polymers with these linkers and different transition metal ions under hydro/solvothermal conditions. A variety of geometries including interpenetrated/non-interpenetrated square grids, distorted (4,4) net, layer, Kagome, diamondoid and self-penetrating 2D and 3D frameworks have been observed and rationalized them with respect to various ligands and reaction conditions used. Variable temperature magnetic susceptibility measurement of one of the compounds is also reported.

Results and discussion

The ligands are chosen such that there is the possibility of rotational motion of arene-imidazole C–N bonds to adopt different conformations and generate different coordination polymer structures.[13] It is known that nitriles can be hydrolyzed to carboxylic acids and ammonia. In neutral conditions, the rate of this reaction is slow, whereas under basic or acidic conditions and high temperatures, the rate of the reaction increases dramatically. Introduction of imidazoles in the ligands can have subtle influences on crystal packing. By judicious control of reaction conditions, ten coordination polymers with different metal ions have been successfully achieved.

The ligands **L4** and **L5** show the characteristic nitrile stretching at $\sim$2230 cm^{-1} in the IR spectra. This peak is absent in the respective coordination polymers[14] and at the same time, each polymer exhibits strong absorption in the region, 1350–1550 cm^{-1} diagnostic of coordinated carboxylate.[15]

Structure of $\{[Cd(L_1)_2]\}_n$, (1)

Single-crystal X-ray analysis reveals that **1** forms a (4,4) grid structure. The metal ion lies on a 2-fold axis, adopts an octahedral geometry with equatorial ligation from four O atoms from two carboxylates bound to the metal in asymmetric chelating fashion (Cd–O, 2.261–2.451 Å) and axial ligation from two imidazole N (Cd–N = 2.261 Å). Thus, each Cd(II) is connected to four different $\mathbf{L_1}^{-1}$ ligands (Fig. 1a). The ligands are bonded to other Cd(II) centers generating a square-grid (4, 4) net as a 2D sheet (Fig. 1b). The grid size of 16.53 × 16.44 Å^2 and the two independent angles of 104.69 and 113.05° are described by a 40-membered $Cd_4(L_1)_4$ macrocyclic ring.

Two such square grid sheets interpenetrate in a parallel manner (Fig. 2a) such that the Cd atom of one layer is located in middle of the grid of the second interpenetrating layer. These 2D interpenetrated sheets stack in —AA— fashion through noncovalent interactions to form an overall 3D structure. There is no open channel and no solvent molecules are found in the lattice of **1** (Fig. 2b).

Structure of $\{[Cu(L_1)_2]\}_n$, (2)

Single-crystal X-ray analysis reveals that **2** has a Kagome structure[16] with 1D hexagonal open channels. Here, the

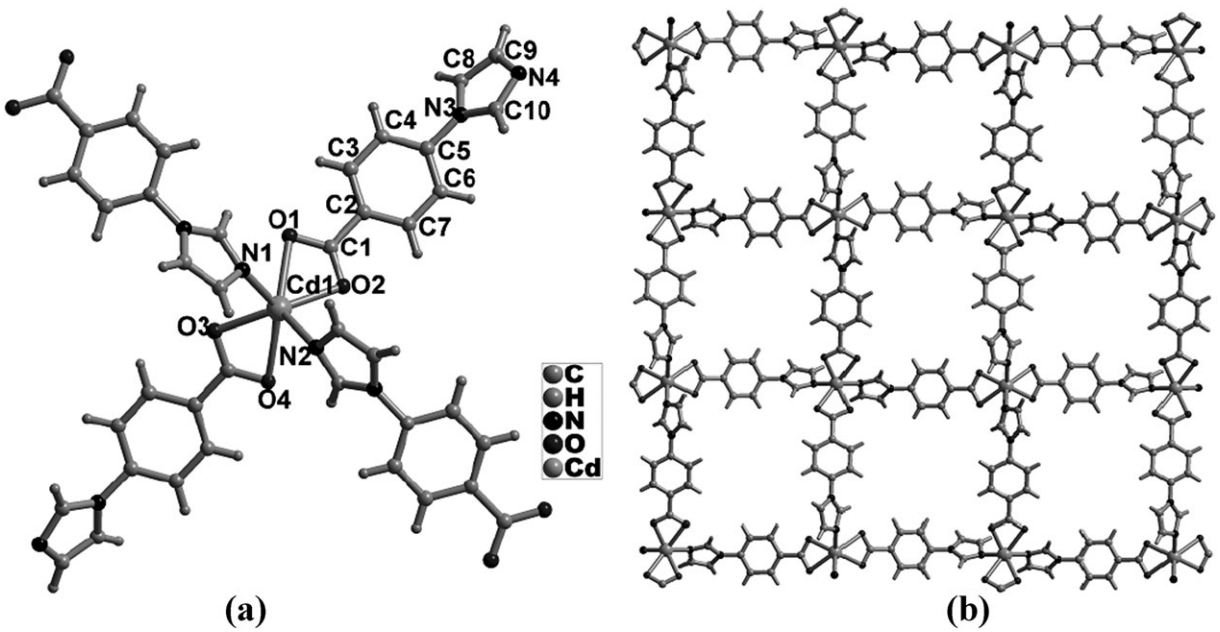

Fig. 1 (a) Coordination environment around Cd(II) center in **1** and (b) View of the single (4,4) net.

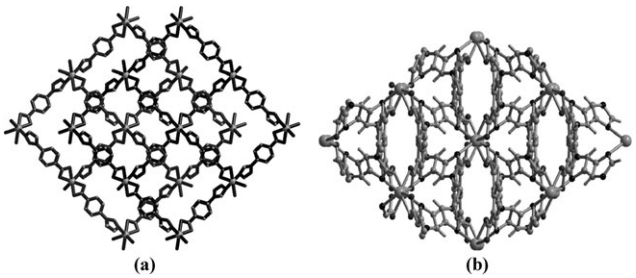

Fig. 2 (a) Schematic view of the parallel 2-fold and (b) Crystal packing along *b*-axis in **1**.

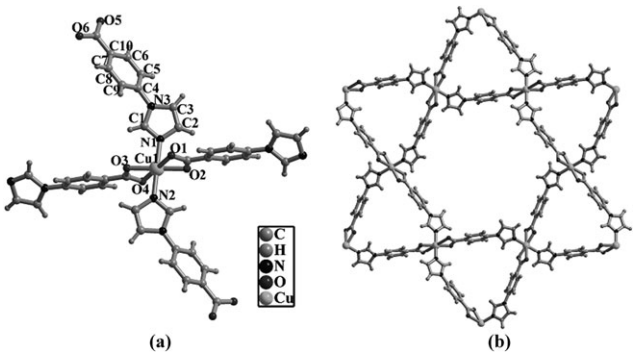

Fig. 3 (a) Coordination environment around Cu(II) center in **2** and (b) View of the 2D Kagome net.

asymmetric unit contains one Cu(II) ion (half occupancy) and one $\mathbf{L_1}^{-1}$. Like in the case of **1**, distorted octahedral Cu(II) is coordinated by two imidazole N (Cu–N = 1.978 Å) and two asymmetrically chelated carboxylates (Cu–O = 1.971–2.663 Å) from four different organic $\mathbf{L_1}^{-1}$ ligands (Fig. 3a). Each Cu(II) ions lie on an inversion center, has four Cu(II) ions as neighbors to generate a Kagome net as a two dimensional sheet showing Cu...Cu distances of 11.747 Å (length of arms) and 23.494 Å as the diagonal Cu...Cu distance in the hexagonal rings (Fig. 3b).

These 2D layers stack over each other in —ABCABC— fashion to generate a three dimensional structure with open channels when viewed along *c*-axis (Fig. 4). The solvent accessible volume for **2**, calculated with the PLATON[17] program, is 20.4% of the total unit cell volume. In a recent report[18] a Kagome structure has been reported with Cu(II) and the present ligand with subtle differences.

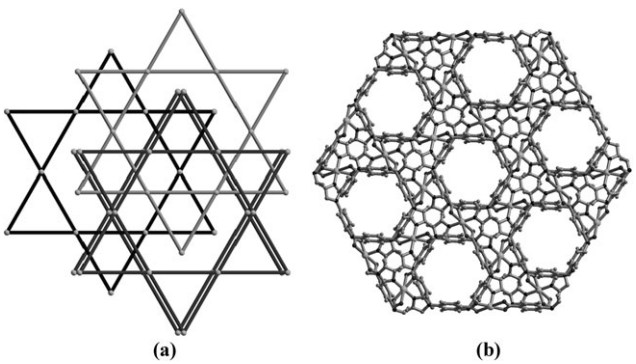

Fig. 4 (a) Schematic representation of —ABCABC— stacking of Kagome layers and (b) Crystal packing along *c*-axis with 1D channels in **2**.

Structure of $\{[Cd_2(L_1)_2(HCOO)_2(H_2O)]\}_n$, (3)

Compound **3** is a 3D mixed ligand coordination polymer with *in situ* generated formate anions. Single-crystal X-ray analysis reveals two crystallographically independent Cd(II) ions, two $\mathbf{L_1}^{-1}$, two formate anions and one coordinated water molecule in the asymmetric unit. The formate comes from the hydrolysis of DMF under high pressure and temperature, which has been widely reported in the literature.[19] The two Cd(II) ions (both octahedral) are bridged by carboxylate to form a bimetallic unit (Cd1—Cd2 separation, ~3.692 Å) and are further connected by two $\mathbf{L_1}^{-1}$ ligands to generate a zig-zag chain along the crystallographic *b*-axis (Fig. 5). The Cd–O and Cd–N bond distances are normal within statistical errors when compared with reported values.[20]

This structure shows two bridging modes of formate anions in a single structure with a rare mono-bridging mode. The zig-zag chains are connected with (*syn*, *anti*) formate anions in both crystallographic *a* and *c* directions to generate a 3D coordination polymer with no embedded guest molecules (Fig. 6).

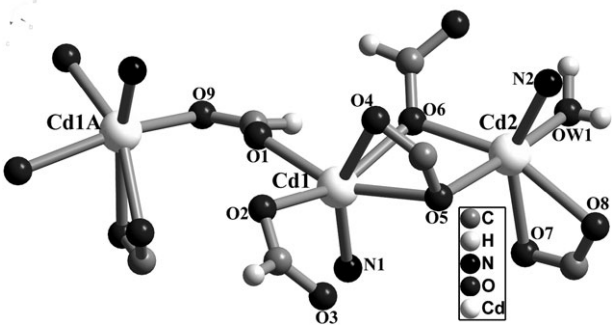

Fig. 5 Coordination environment around Cd(II) center in **3** (only partial $\mathbf{L_1}^{-1}$ are given for clarity).

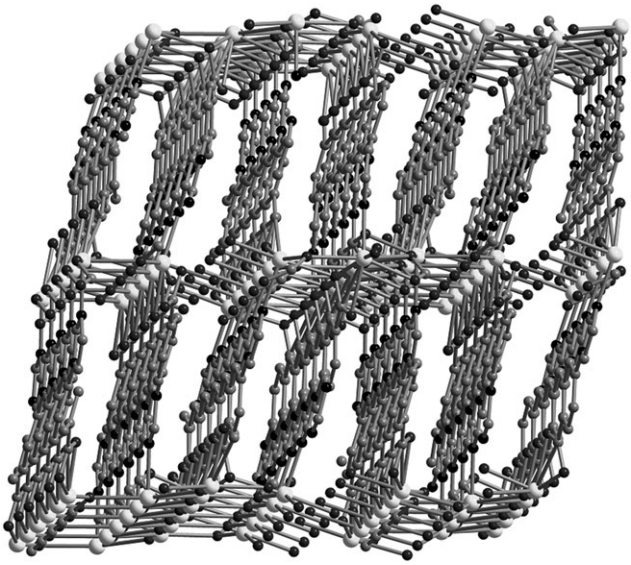

Fig. 6 Crystal packing along *b*-axis in **3**.

Structure of $\{[Cd_2(L_1)_4]\cdot 3H_2O\}_n$, (4)

This compound crystallizes in the chiral triclinic space group P1. The asymmetric unit contains two Cd(II) ions, four L_1^{-1} and three water molecules. In this structure, each metal ion shows a distorted octahedral geometry (Fig. 7a) with ligation from two chelating carboxylates (Cd–O, 2.333–2.417 Å) and two imidazole nitrogens (Cd–N, 2.256–2.276 Å) to form an adamantane type architecture containing 10 Cd(II) ions and 12 L_1^{-1} ligands (Fig. 7b).

The generated adamantanoid moieties make 4-fold interpenetration, although the resulting 3D network contains voids that are filled with guest water molecules (Fig. 8).

While these water molecules are H-bonded to the neighboring carboxylate O (~2.8 Å), weak π...π stacking interactions between aromatic moieties are also present. The solvent accessible volume for **4**, calculated by PLATON as 21.2% of the total unit cell volume.

Structure of $\{[Cd(L_1)(CH_3COO)]\}_n$, (5)

The asymmetric unit here contains two crystallographically independent Cd(II) ions (both half occupancy) lie on the same 2-fold axis, one L_1^{-1} and one acetate. One of the metal ions is distorted octahedrally coordinated with equatorial ligation by two chelating carboxylates (Cd–O, 2.321–2.373 Å) and axial ligation by two imidazole nitrogens (Cd–N, 2.253 Å). The other metal ion shows 8-coordination with ligation from four chelating carboxylates (Cd–O, 2.228–2.764 Å) (Fig. 9a). The polyhedra generated around Cd(II) centers are shown in Fig. 9b.

This dinuclear motif is repeated along *b*-axis to generate a 1D chain that is further connected with L_1^{-1} linkers to form a 2D coordination polymer (Fig. 10a). Also, stacking of these 2D layers one over the other in —ABCDE— fashion generates a packed 3D supramolecular architecture (Fig. 10b).

Structure of $\{[Cd(L_1)_2(C_5H_5N)]\cdot 2.5H_2O\}_n$, (6)

This compound crystallizes in the non-centrosymmetric tetragonal space group $P4_32_12$. The asymmetric unit contains one

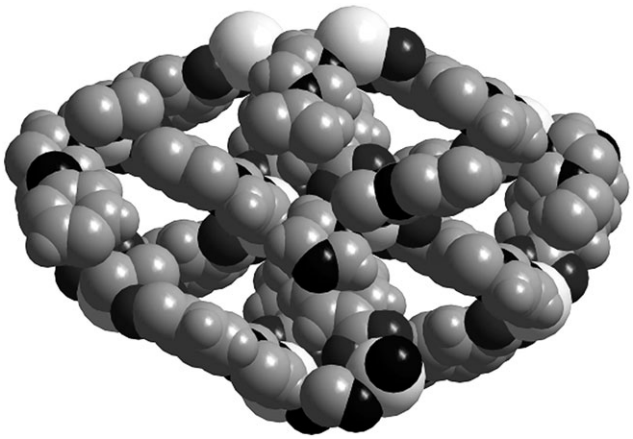

Fig. 8 View of the 3D structure along *a*-axis with open channels in **4** (guest water molecules in channels are omitted for clarity).

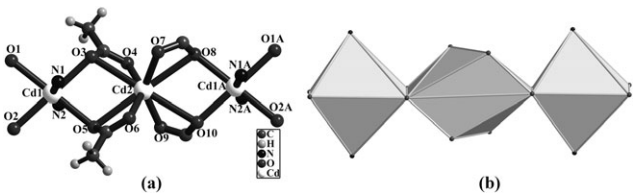

Fig. 9 (a) Coordination environment around Cd(II) centers and (b) Polyhedra generated around metal centers in **5**.

Cd(II) (half occupancy), one L_1^{-1}, half of the pyridine and 1.25 water molecules. Cd(II) ion and distorted pyridine molecule lie on the same 2-fold axis. The metal ion shows distorted pentagonal bipyramidal geometry (Fig. 11) with bonding from two chelating carboxylates (Cd–O, 2.400–2.488 Å), two imidazole N (Cd–N, 2.279 Å) and the pyridine N (Cd–N, 2.328 Å).

The network structure of **6** is similar to that of **4** except that octahedral Cd(II) is replaced by pentagonal bipyramidal Cd(II) (Fig. 12a). Interestingly, the diamondoid network possesses 3-fold interpenetration instead of 4-fold due to the

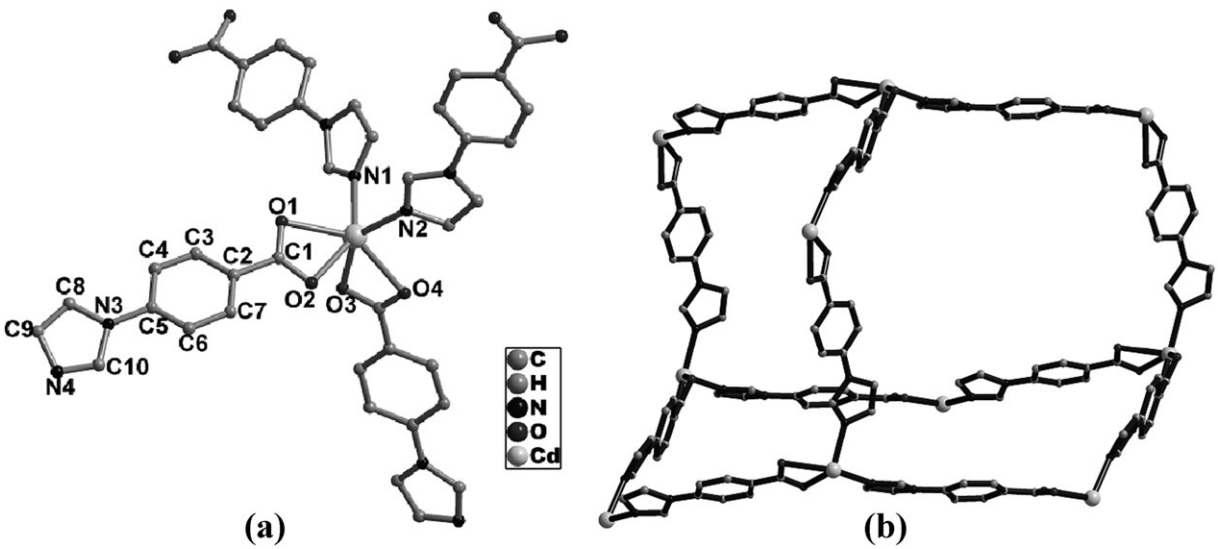

Fig. 7 (a) Coordination environment around Cd(II) center in **4** and (b) View of the single adamantane composed of $Cd_{10}L_{1(12)}$ unit in **4**.

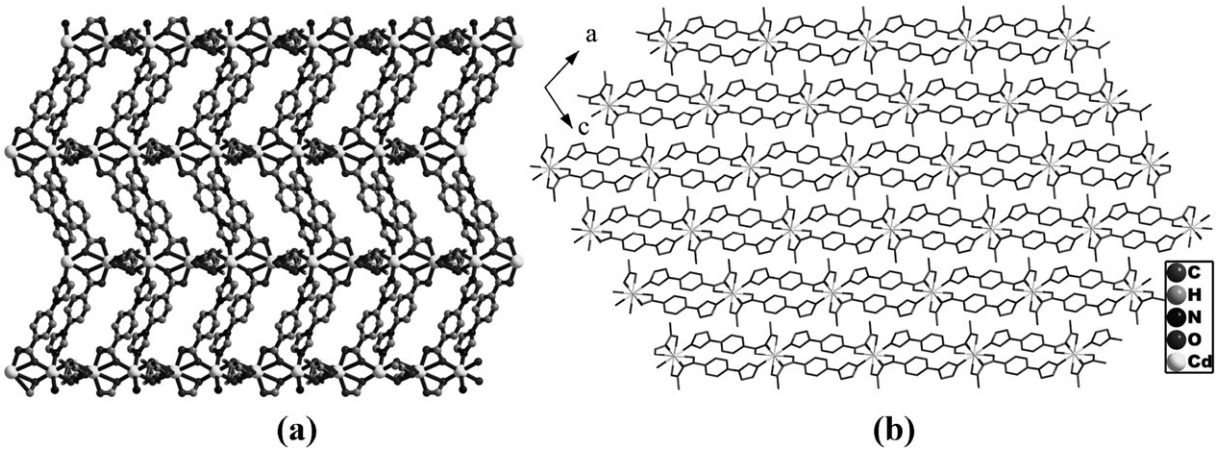

Fig. 10 (a) View of the single 2D network and (b) Crystal packing along *b*-axis in **5**.

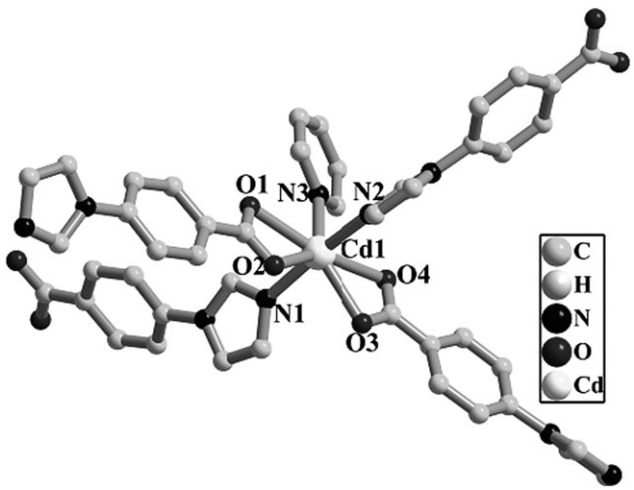

Fig. 11 Coordination environment around Cd(II) center in **6**.

coordinated pyridine molecules which itself occupy some of the space in spacious single net. Fig. 12b shows how coordinated pyridine molecules occupy the voids in the framework.

Structure of $\{[Zn(L_2)_2]\}_n$, (7)

This compound crystallizes in the non-centrosymmetric orthorhombic space group Aba2. The asymmetric unit contains one Zn(II) and two $\mathbf{L_2}^{-1}$ ligands. The $\mathbf{L_2}^{-1}$ ligands are generated through hydrolysis during hydrothermal reaction. The metal ion shows distorted tetrahedral coordination with bonding from two monodentate carboxylate and two imidazole N (Fig. 13).

All Zn–O and Zn–N bond distances are within normal statistical errors[21] as found in other Zn(II) complexes. Zn(II) ions along with the ligand $\mathbf{L_2}^{-1}$ form a $Zn_6(L_2)_6$ macrocycle in the form of an open-book. These macrocyclic units form a parallel self-interpenetrated 2D network (Fig. 14). These independent

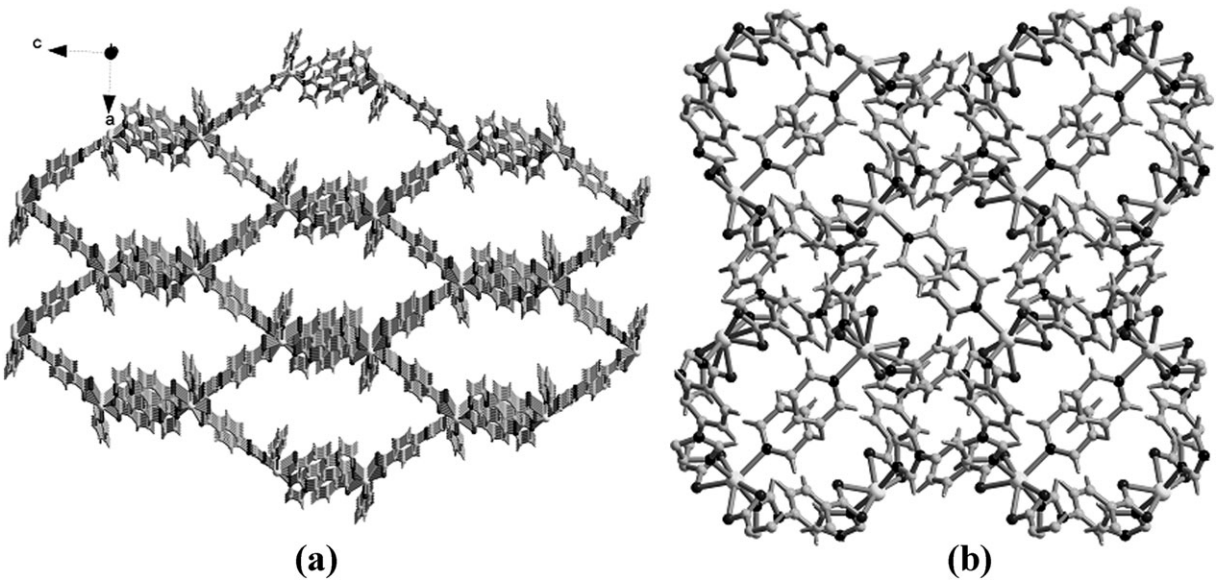

Fig. 12 (a) A single diamondoid framework and (b) 3D structure along *c*-axis where channels are occupied by coordinated pyridine molecules in **6**.

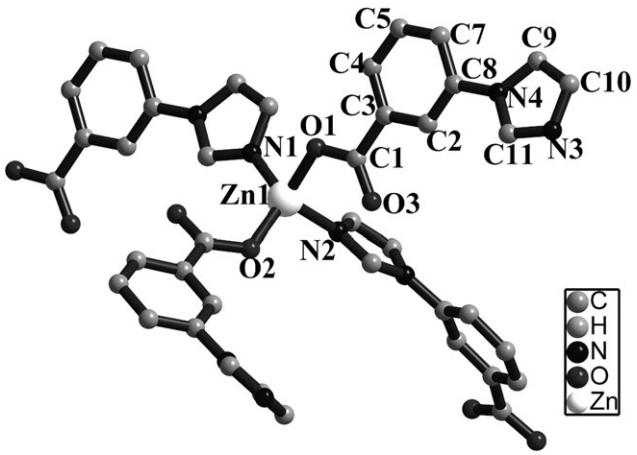

Fig. 13 Coordination environment around Zn(II) center in **7**.

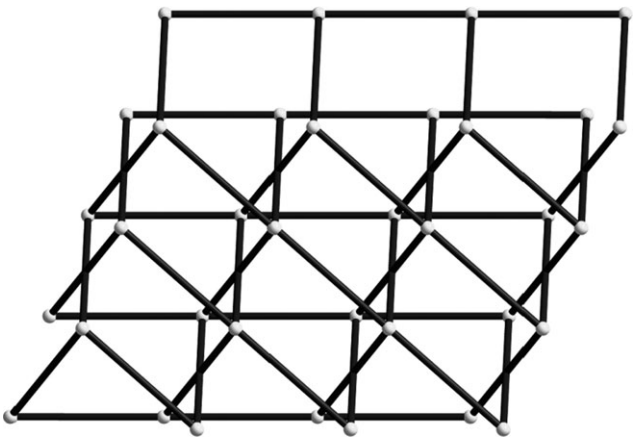

Fig. 14 Single self-penetrating 2D sheet in **7**.

2D networks stack in —ABAB— fashion to generate an overall 3D structure.

As reported by Sun *et al.*[9d] Zn(II) polymer with $\mathbf{HL_1}$ is a 2D interpenetrated (4,4) net, *meta*-substituted analogue $\mathbf{HL_2}$ forms a self-penetrated 2D coordination polymer. Still we have tried same experimental methods in both cases but did not able to get self-penetrated structure with $\mathbf{L_1}$ which confirm the crucial role of the nature of organic ligands to obtain specific supramolecular structures. While few 3D self-penetrated structures are known[22] in the literature, self-penetrated 2D coordination polymers are still rare.[23]

Structure of $\{[Cd_2(L_2)_4]\cdot H_2O\}_n$, (8)

Compound **8** crystallizes in the monoclinic space group $P2_1/c$ as a non-interpenetrated 2D net. The asymmetric unit contains two Cd(II) ions, four $\mathbf{L_2}^{-1}$ and one water molecule. Each metal ion is distorted octahedral with coordination from two chelating carboxylates and two imidazole N (Fig. 15). The overall structure is a (4,4) net having the grid size (considering diagonals of two opposite metal centers) of 17.5×10.7 Å^2 (Fig. 16).

Two different types of interactions and spacing exist in between layers. As shown in Fig. 17, two layers composed of

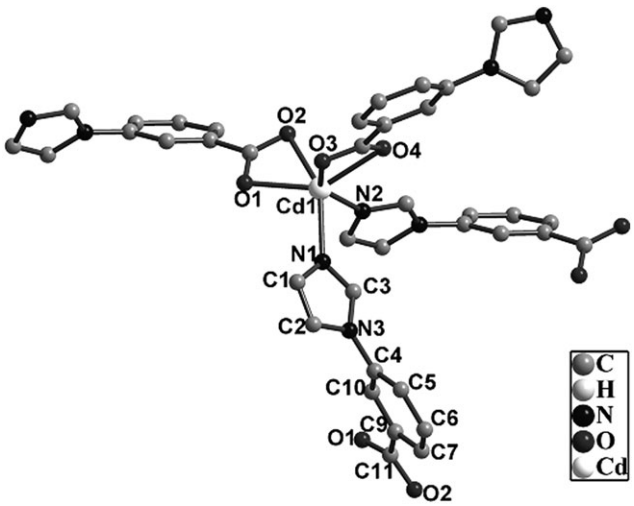

Fig. 15 Coordination environment around Cd(II) center in **8**.

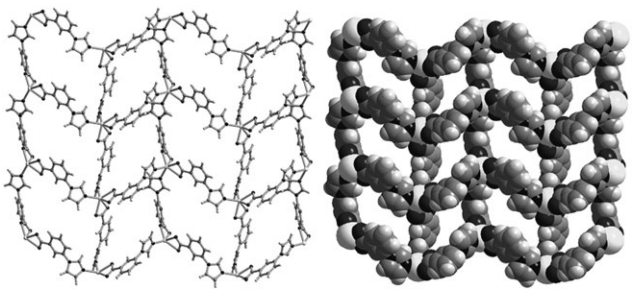

Fig. 16 (a) Single (4,4) net in **8** and (b) Space filling model of that net.

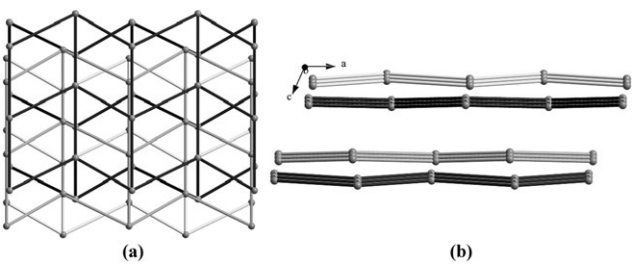

Fig. 17 Schematic view of the (a) stacking of layers and (b) non-interpenetrating layer structure along *b*-axis in **8**.

identical nets stacked over one another in —ABAB— fashion are held together by week π...π interactions (~3.7 Å) with an interlayer spacing of ~3.6 Å calculated by considering the van der Waals radii of atoms. These two 2D-layers are further stacked in —ABAB— fashion and connected through H-bonds with coordinated carboxylate O atoms and trapped water molecules (OW1–O, 2.813–2.874 Å), where the spacing between two sets of the layers is ~4.2 Å to generate an overall 3D structure.

On comparison with the structure of **1** which is double interpenetrated, **8** is non-interpenetrated presumably due to the angular nature of the donor atoms in $\mathbf{L_2}^{-1}$. Also, strong π...π interactions between aromatic rings of two layers in **8** can stabilize the structure without interpenetration.

Structure of $\{[Cd_3(L_2)_6(H_2O)]\cdot 2EtOH\cdot H_2O\}_n$, (9)

The asymmetric unit in this structure contains three crystallographically independent Cd(II), six L_2^{-1} ligands, one metal bound water molecule besides one water and two ethanol molecules in the lattice. Each Cd(II) ion shows a different coordination geometry. Distorted octahedral Cd(1) is bonded equatorially to two bridging carboxylates (Cd1–O, 2.206–2.776 Å) and axially to two imidazole N (Cd1–N, 2.210–2.279 Å) from four different ligand moieties. The Cd(2) is 7-coordinated with two chelating carboxylates (Cd2–O, 2.275–2.523 Å), one bridging carboxylate (Cd2–O, 2.805 Å) and two imidazole nitrogens (Cd2–N, 2.264–2.296 Å). The third Cd(II) ion is bonded to two chelating carboxylates (Cd3–O, 2.351–2.511 Å), two imidazole N (Cd3–N, 2.304–2.309 Å) and one water molecule (Cd3–OW1, 2.296 Å) (Fig. 18a).

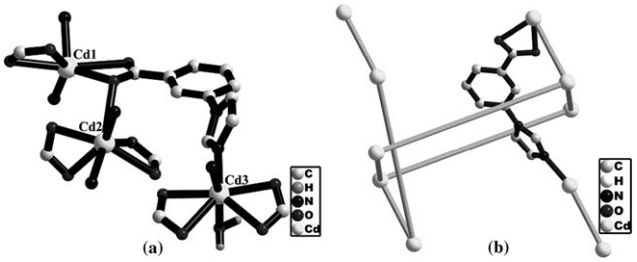

Fig. 18 (a) Coordination environment around Cd(II) centers. (b) View of the self-penetration in the 3D structure of **9**.

Overall, the structure is a 3D self-penetrating coordination polymer in which free ethanol and water solvent molecules are trapped. Fig. 18b illustrates how self-penetration occurs in this structure. The angular nature of ligand L_2^{-1} plays a crucial role for self-penetration. It is interesting to note here that pH of the reaction medium has a profound effect on the structure of the coordination polymer, as under basic conditions 2D self-penetrating structure **8** was isolated, and under neutral conditions 3D self-penetrating structure **9** was isolated.

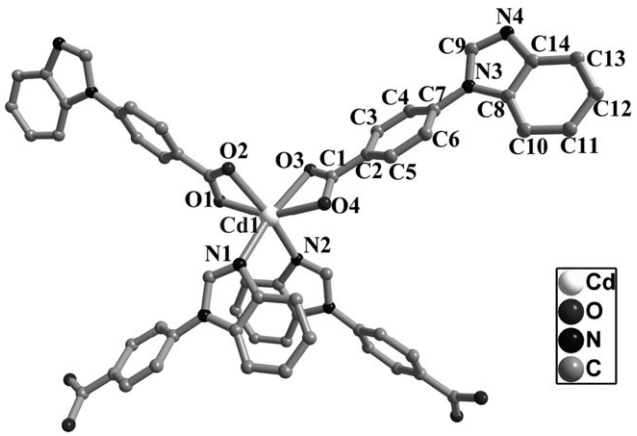

Fig. 19 Coordination environment around Cd(II) center in **10**.

Structure of $\{[Cd(L_3)_2]\cdot 2DMF\cdot 4H_2O\}_n$, (10)

The asymmetric unit in **10** contains one Cd(II) ion which lies on a 2-fold axis, two L_2^{-1} besides one DMF and two water molecules in the lattice. The metal ion is distorted octahedral with coordination from two chelating carboxylates (Cd–O, 2.312–2.372 Å) and two imidazole N (Cd–N, 2.285 Å) (Fig. 19). The overall structure is a 2D coordination polymer with (4,4) net having rhombic grid size of 18.29 × 16.26 $Å^2$ (diagonal) (Fig. 20a).

Due to bulky nature of the benzimidazole moiety and high capacity of π...π stacking with aromatic rings, these 2D layers are stacked one over the other to generate a non-interpenetrated 3D structure with open channels along the *c*-axis. These channels are filled with guest DMF and water molecules (Fig. 20b). The solvent accessible volume for **10**,

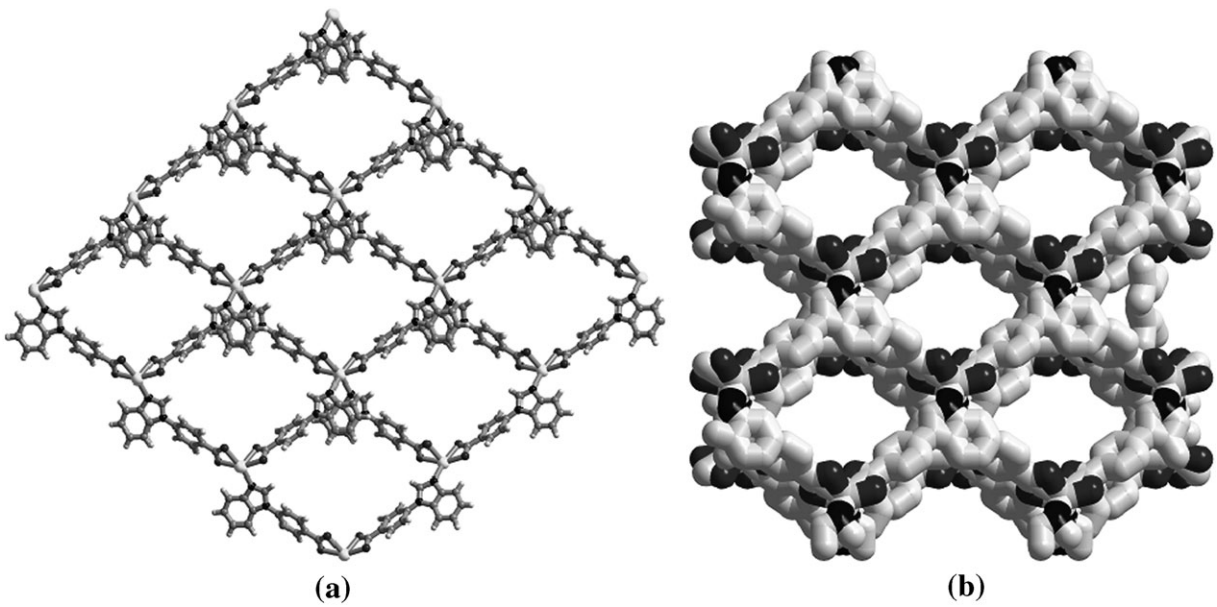

Fig. 20 Schematic view of the (a) 2D layers and (b) space filling model with 1D channels along *c*-axis in **10**.

calculated with the PLATON program, is 41.6% of the total unit cell volume.

It is obvious from the above descriptions that the nature of ligands and reaction conditions has significant effects on the final structures of the resulting complexes. As demonstrated by a comparison of Cd(II) complexes **1** and **8**, doubly interpenetrated and non-interpenetrated (4,4) net were separated with $\mathbf{L_1}^{-1}$ and $\mathbf{L_2}^{-1}$ respectively under neutral and basic conditions. Similarly comparison of Zn(II) complexes of $\mathbf{L_1}^{-1}$ reported by Sun *et al.*[9d] and $\mathbf{L_2}^{-1}$ have doubly interpenetrated and self-penetrated architectures with tetrahedral metal centers. Basically linear and angular nature of $\mathbf{L_1}^{-1}$ and $\mathbf{L_2}^{-1}$ causes the distinctness of the coordination environment around metal centers and finally results in the formation of different structures. Also, angular or bent nature is helpful to stabilize the structure through strong π...π interactions between aromatic rings of two layers and prevent interpenetration. In addition, reaction conditions have a significant effect on the structures, as evidenced by the fact that the structures of **4** and **9** are significantly different, even though the reaction conditions are the same. But under basic conditions, $\mathbf{L_2}^{-1}$ generates (4,4) net structure without interpenetration. It should be noted that we didn't successfully isolate the crystals of $\mathbf{L_2}^{-1}$ with metal ions *via* direct use of $\mathbf{HL_2}$. Under high temperature and pressure the CN functional groups get hydrolyzed slowly to corresponding carboxylic acid and generates the metal bound coordination polymers, which highlights the importance of *in situ* generated ligands. Furthermore, the comparison of **10** with **1** and **8** shows that the increase of bulky and high capacity of π...π stacking in organic ligands may exert an important influence on the formation of resulting diverse structures.

In addition to the aforementioned coordination polymers, we have also tried to synthesize coordination polymers with other transition metal ions under different experimental conditions, but only Zn(II) and Co(II) bound coordination polymers of $\mathbf{L_1}^{-1}$ were separated. These structures have the same doubly interpenetrated (4,4) net structures as **1** with tetrahedrally coordinated metal centers as reported in the literature, while other cases generate amorphous powders with unknown compositions.

Thermogravimetric analysis

In order to examine thermal stabilities of these compounds, TG analyses are carried out in N_2 atmosphere at the rate of 5 °C per minute. The thermograms are shown in the Supporting Information‡.[14] The TGA curves of **1**, **2**, **5** and **7** show no weight loss and they decompose at various temperatures but not before 400 °C. Compound **3** shows a weight loss of 2.5% due to removal of one H_2O molecule (calculated, 2.54%) and starts to decompose at ~290 °C. Compound **4**, on the other hand, shows a weight loss of 5.5% due to removal of $3H_2O$ (calculated, 5.26%) and the framework starts to decompose at ~310 °C. Compound **6** shows a weight loss in stages – first a loss of 6% due to $3H_2O$ starting at 80 °C and then a loss of ~16% starting at 290 °C due to metal-bound pyridine. The framework starts to decompose at ~310 °C as coordinated pyridine molecule is liberated. TGA of compound **8** shows a weight loss of 2.0% corresponding to one water molecule (calculated, 1.8%) and the 2D framework is stable up to 350 °C. Compound **9** shows a weight loss of 8.0% (calculated, 7.0%) corresponding to $2C_2H_5OH + H_2O$ starting at 90 °C and continuing up to ~300 °C. The framework is stable up to ~380 °C. Finally, compound **10** shows weight loss in two stages beginning at 50 °C and continuing up to 180 °C showing a total loss of 29% (calculated, 27%) corresponding to two DMF and four water molecules. The framework is, however, stable up to ~360 °C.

Magnetic properties

Variable temperature magnetic susceptibility data for compound **2** are collected with an applied DC field of 1.0 T in the 2 to 300 K temperature range. The χT product at 300 K has a value of 0.39 cm^3 K mol^{-1} per Cu(II) ion, in agreement with the value expected for an isolated Cu(II) ion (χT = 0.375 cm^3 K mol^{-1} at 300 K, S = 1/2 and g = 2.0). As temperature decreases, the χT product (circles in Fig. 21) remains nearly constant, and then decreases sharply at temperatures below 10 K.

This indicates that the Cu(II) ions in **2** are magnetically isolated from their neighbours in the solid state. This is not surprising and can be expected from the structure of compound **2**. The Cu(II) ions are bridged by the ligand at a

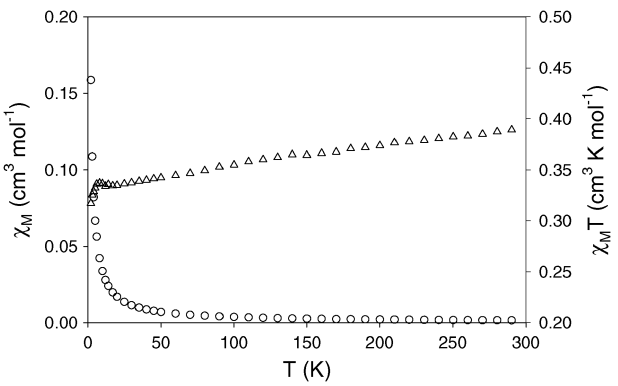

Fig. 21 Temperature dependence of the magnetic susceptibility for compound **2**.

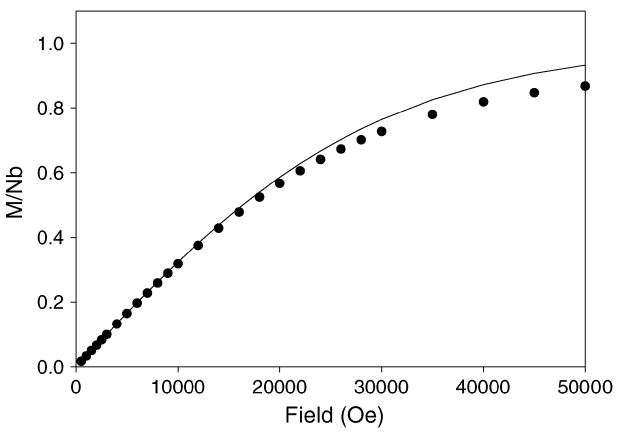

Fig. 22 Field dependence of the magnetization for compound **2**. The solid line is the Brillouin curve for S = 1/2 and g = 2.0.

distance of 11.747 Å. Fig. 22 shows field dependence of magnetization which follows the Brillouin law, as expected for an isolated Cu(II).

Conclusion

We have utilized rigid ditopic organic linkers for the synthesis of ten coordination polymers with different metal ions. These ditopic ligands have a strong ability to bind with metal ions and tendency to show the flexibility that can generate a variety of supramolecular architecture. The nature of the metal ions and organic ligands is the key to synthesize these polymers, even using similar conditions. We have shown interpenetrated/noninterpenetrated (4,4) nets, Kagome net, 3-fold and 4-fold diamondoid nets and self-penetrating 2D and 3D nets with complete structural characterization. Interesting self-penetrating 2D and 3D polymers were separated under *in situ* cyanide hydrolysis and structural comparison was demonstrated with similar type of ligands.

Experimental

Materials and methods

Ethyl-4-fluorobenzoate, 4-fluorobenzonitrile, ethyl-3-fluorobenzoate, 3-fluorobenzonitrile and metal salts were purchased from Aldrich and used as received. All solvents, imidazole, benzimidazole and K_2CO_3 were procured from S. D. Fine Chemicals, India. All solvents were purified prior to use.

Physical measurements

Infrared spectra were recorded on a Perkin-Elmer Model 1320 spectrometer (KBr disk, 400–4000 cm^{-1}). ^{1}H-NMR were recorded on a JEOL JNM-LA500 FT (500 MHz) instrument in DMSO-d^6 with Me_4Si as the internal standard. ESI mass spectra were recorded on a WATERS Q-TOF Premier mass spectrometer. X-Ray powder patterns were obtained using a Phillips PW 100 X-ray generator (Cu-Kα radiation at a scan rate of 3°/min, 293 K), while thermogravimetric analyses (TGA) were carried out on a Mettler Toledo thermal analyzer (heating rate of 5 °C min^{-1}). Microanalyses for the compounds were carried out using a CE-440 elemental analyzer (Exeter Analytical Inc.).

Magnetic susceptibility data (2–300 K) were collected at the Unitat de Mesures Magnètiques at the Universitat de Barcelona using crushed crystals of the sample on a Quantum Design MPMS-XL SQUID magnetometer equipped with a 5T magnet. The data were corrected for temperature independent paramagnetism (TIP) and the diamagnetic corrections were calculated using Pascal's constants; an experimental correction for the sample holder was applied.

Synthesis

All syntheses were carried out in dinitrogen atmosphere unless otherwise mentioned.

Synthesis of 4-imidazole-1-yl-benzoic acid (HL_1). This ligand was synthesized following a reported procedure.[12]

Synthesis of 3-imidazole-1-yl-benzoic acid (HL_2). This compound was synthesized similar to HL_1. A mixture containing imidazole (1.1 mmol), ethyl-3-fluorobenzoate (1 mmol) and K_2CO_3 (1.5 mmol) in 10 mL of *N*,*N*′-dimethyl formamide (DMF) was heated at 100 °C for 48 h with constant stirring. After removal of solvent under reduced pressure, the residue was washed with water and the compound extracted with ethyl acetate. Removal of ethyl acetate afforded a colorless oily product as the ester. It was hydrolyzed by boiling in 5% aqueous ethanolic NaOH solution for 10 h. Acidification with 1N HCl afforded the desired acid as a white solid which was washed several times with water and dried in air. Yield: 63%.

Synthesis of 4-benzmidazole-1-yl-benzoic acid (HL_3). The ligand HL_3 was synthesized adopting a procedure as in case of HL_2. A mixture of benzimidazole (1.1 mmol), ethyl-4-fluorobenzoate (1 mmol) and K_2CO_3 (1.5 mmol) in 10 mL of DMF were heated at 100 °C for 48 h with constant stirring. Thereafter, all the solvent was removed under reduced pressure, the residue was washed with water and the compound extracted with ethyl acetate. Removal of ethyl acetate afforded a crude product that was recrystallized from methanol to obtain the ester as a pale yellow crystalline solid. The acid was obtained by hydrolyzing the ethyl ester in aqueous ethanol containing 5% NaOH followed by acidification with 1N HCl. The desired acid precipitates as a pale-brown solid. Yield: 71%. ^{1}H-NMR, δ (ppm): 8.6 (s, 1H), 8.13–8.12 (d, 2H), 7.8–7.78 (d, 2H), 7.76–7.74 (d, 1H), 7.69–7.68(d, 1H), 7.35–7.29 (q, 2H).

Synthesis of 4-imidazole-1-yl-benzonitile (L_4). This ligand was synthesized following a reported procedure.[24]

Synthesis of 3-imidazole-1-yl-benzonitile (L_5). A mixture of imidazole (1.1 mmol), 3-fluorobenzonitrile (1 mmol) and K_2CO_3 (1.5 mmol) in 10 mL of DMF were heated at 100 °C for 48 h with constant stirring. After cooling to room temperature, the mixture was poured slowly into ice-water (100 ml) with constant stirring. The precipitated white solid was collected by filtration, washed with water and dried in air. The crude product was recrystallized from methanol to get needle like crystals. Yield: 46%. ^{1}H-NMR, δ (ppm): 8.4 (s, 1H), 8.18 (s, 1H), 7.98–7.96 (dd, 1H), 7.8 (s, 1H), 7.77–7.75(d, 1H), 7.68–7.65 (t, 1H), 7.09 (s, 1H); ESI-MS: m/z (80%) 170.0673 $[M + 1]^+$.

Synthesis of $\{[Cd(L_1)_2]\}_n$, (1). A mixture of $Cd(NO_3)_2{\cdot}6H_2O$ (0.50 mmol) and HL_1 (0.25 mmol) in H_2O (4 ml) was placed in a Teflon-lined stainless steel autoclave, and heated to 180 °C for 72 h. After the mixture was cooled to room temperature at the rate of 0.1 °C min^{-1}, colorless crystals of **1** were collected, washed with water and dried at room temperature to give 38% yield based on $Cd(NO_3)_2{\cdot}6H_2O$. Anal. calcd. for **1**: C, 49.35%; H, 2.89%; N,11.51%. Found: C, 49.13%; H, 3.01%; N,11.73%. IR (cm^{-1}): 3134(s), 1604(m), 1548(m), 1394(m), 1302(s), 1237(s), 1169(s), 1116(m), 1061(m), 1015(s), 962(s), 931(s), 852(m), 832(s), 783(m), 748(s), 721(s), 699(s), 656(m).

Synthesis of $\{[Cu(L_1)_2]\}_n$, (2). A mixture of $Cu(NO_3)_2{\cdot}6H_2O$ (0.50 mmol), 4-imidazole-1-yl-benzoic acid ethyl ester[12] (0.25 mmol) and aq. NH_3 (0.1 ml) in dist. H_2O (4 ml) were

placed in a Teflon-lined stainless steel autoclave and heated to 180 °C for 72 h. After the mixture was cooled to room temperature at the rate of 0.1 °C min^{-1}, colorless crystals of **2** were collected, washed with water and dried at room temperature to give 31% yield based on $Cu(NO_3)_2{\cdot}6H_2O$. Anal. calcd. for **2**: C, 54.85%; H, 3.22%; N, 12.79%. Found: C, 55.17%; H, 3.41%; N, 12.47%. IR (cm^{-1}): 3164(w), 3143(s), 2923(w), 1689(m), 1689(s), 1609(w), 1577(s), 1500(m), 1421(s), 1361(m), 1273(m), 1230(m), 1177(m), 1150(m), 1133(m), 1119(m), 1096(m), 1062(m), 964(m), 948(m), 875(s),846(m), 782(m), 745(m), 700(s), 660(s), 644(s).

Synthesis of $\{[Cd_2(L_1)_2(HCOO)_2(H_2O)]\}_n$, (3). A mixture of $Cd(NO_3)_2{\cdot}6H_2O$ (0.50 mmol) and HL_1 (0.25 mmol) in DMF–H_2O (4 ml, 3 : 1 v/v) were placed in a Teflon-lined stainless steel autoclave and heated to 110 °C for 48 h. After the mixture was cooled to room temperature at the rate of 0.1 °C min^{-1}, colorless crystals of **3** were collected, washed with water and dried at room temperature to give 49% yield based on $Cd(NO_3)_2{\cdot}6H_2O$. Anal. calcd. for **3**: C, 37.36%; H, 2.56%; N, 7.92%. Found: C, 37.27%; H, 2.68%; N, 7.77%. IR (cm^{-1}): 3398(br), 3124(m), 1606(s), 1568(w), 1523(m), 1402(s), 1308(m), 1267(w), 1188(w), 1121(m), 1062(m), 961(m), 932(w), 857(m), 782(s), 746(w), 695(w), 643(m).

Synthesis of $\{[Cd_2(L_1)_4]{\cdot}3H_2O\}_n$, (4). A mixture of $Cd(NO_3)_2{\cdot}6H_2O$ (0.50 mmol) and L_4 (0.25 mmol) in EtOH–H_2O (4 ml, 1 : 1 v/v) were placed in a Teflon-lined stainless steel autoclave and heated to 180 °C for 72 h. After the mixture was cooled to room temperature at the rate of 0.1 °C min^{-1}, colorless crystals of **4** were collected, washed with water and dried at room temperature to give 13% yield based on $Cd(NO_3)_2{\cdot}6H_2O$. Anal. calcd. for **4**: C, 46.75%; H, 3.33%; N, 10.90%. Found: C, 46.92%; H, 3.42%; N, 10.76%. IR (cm^{-1}): 3403(br), 3134(m), 1607(s), 1549(m), 1524(m), 1402(s), 1304(m), 1263(m), 12185(m), 1063(s), 1014(w), 963(m), 934(w), 857(m), 783(m), 740(w), 697(w), 650(w).

Synthesis of $\{[Cd(L_1)(CH_3COO)]\}_n$, (5). A mixture of $Cd(OAc)_2{\cdot}6H_2O$ (0.50 mmol), **L_4** (0.25 mmol) and aq. NH_3 (0.1 ml) in EtOH–H_2O (4 ml, 1:1v/v) were placed in a Teflon-lined stainless steel autoclave and heated to 180 °C for 72 h. After the mixture was cooled to room temperature at the rate of 0.1 °C min^{-1}, colorless crystals of **5** were collected, washed with water and dried at room temperature to give 42% yield based on $Cd(NO_3)_2{\cdot}6H_2O$. Anal. calcd. for **5**: C, 40.18%; H, 2.81%; N, 7.81%. Found: C, 40.03%; H, 2.93%; N, 7.91%. IR (cm^{-1}): 3107(s), 2928(s), 1606(m), 1537(s), 1511(s), 1418(m), 1345(s), 1305(s), 1261(s), 1224(m), 1172(m), 1106(s), 1067(m), 855(s), 820(s), 781(m), 728(s), 698(s), 640(m).

Synthesis of $\{[Cd(L_1)_2(C_5H_5N)]{\cdot}2.5H_2O\}_n$, (6). Hot DMF solution of HL_1 (0.25 mmol, 5 ml) and pyridine (0.1 ml) were added slowly into a hot aqueous solution of $Cd(NO_3)_2{\cdot}6H_2O$ (0.50 mmol in 2 ml H_2O) with constant stirring. The mixture left stirring at room temperature for 2 h. Then the solution was filtered and the filtrate left for crystallization. Colorless crystals of **6** were collected after 10 days in 29% yield based on $Cd(NO_3)_2{\cdot}6H_2O$. Anal. calcd. for **6**: C, 48.43%; H, 4.06%; N, 11.29%. Found: C, 48.66%; H, 3.92%; N, 11.15%. IR (cm^{-1}): 3578(w,br), 3360(s), 2985(s), 1585(m), 1539(s), 1481(s), 1391(m), 1240(m), 1211(m), 1163(m), 1012(s), 976(m), 924(s), 852(m), 800(m), 780(m), 749(m), 718(m), 641(s).

Synthesis of $\{[Zn(L_2)_2]\}_n$, (7). A mixture of $Zn(NO_3)_2{\cdot}6H_2O$ (0.50 mmol) and L_5 (0.25 mmol) in H_2O (4 ml) were placed in a Teflon-lined stainless steel autoclave and heated to 180 °C for 72 h. After the mixture was cooled to room temperature at the rate of 0.1 °C min^{-1}, colorless crystals of **7** were collected, washed with water and dried at room temperature to obtain 30% yield of the product based on $Zn(NO_3)_2{\cdot}6H_2O$. Anal. calcd. for **7**: C, 54.62%; H, 3.20%; N, 12.74%. Found: C, 54.46%; H, 3.39%; N, 12.50%. IR (cm^{-1}): 3147(w), 3123(m), 3065(w), 3037((w), 1620(s), 1583(s), 1515(s), 1452(m), 1375(s), 1352(s), 1243(m), 1144(m), 1066(s), 989(w), 947(s), 901(m), 858(m), 823(m), 766(s), 732(s), 684(s).

Synthesis of $\{[Cd_2(L_2)_4]{\cdot}H_2O\}_n$, (8). A mixture of $Cd(NO_3)_2{\cdot}6H_2O$ (0.50 mmol), L_5 (0.25 mmol) and aq. NH_3 (0.1 ml) in EtOH–H_2O (4 ml, 1 : 1 v/v) were placed in a Teflon-lined stainless steel autoclave and heated to 180 °C for 72 h. After the mixture was cooled to room temperature at the rate of 0.1 °C min^{-1}, colorless crystals of **8** were collected, washed with water and dried at room temperature to get 44% yield based on $Cd(NO_3)_2{\cdot}6H_2O$. Anal. calcd. for **8**: C, 48.45%; H, 3.04%; N, 11.30%. Found: 48.51%; H, 2.91%; N, 11.46%. IR (cm^{-1}): 3141(s), 3101(s), 1577(m), 1512(m), 1447(m), 1397(m), 1325(s), 1247(m), 1115(m), 1064(m), 989(s), 935(m), 868(m), 824(m), 771(m), 736(m), 689(m), 651(m).

Synthesis of $\{[Cd_3(L_2)_6(H_2O)]{\cdot}2EtOH{\cdot}H_2O\}_n$, (9). A mixture of $Cd(NO_3)_2{\cdot}6H_2O$ (0.50 mmol) and L_5 (0.25 mmol) in EtOH–H_2O (4 ml, 1 : 1 v/v) were placed in a Teflon-lined stainless steel autoclave and heated to 180 °C for 72 h. After the mixture was cooled to room temperature at the rate of 0.1 °C min^{-1}, colorless crystals of **9** were collected, washed with water and dried at room temperature to give 35% yield based on $Zn(NO_3)_2{\cdot}6H_2O$. Anal. calcd. for **9**: C, 48.39%; H, 3.68%; N, 10.58%. Found: C, 48.22%; H, 3.49%; N, 10.43%. IR (cm^{-1}): 3401(w,br), 3111(s), 1554(m), 1511(s), 1448(s), 1396(m), 1261(s), 1115(s), 1063(m), 933(s), 867(s), 828(s), 772(m), 734(m), 688(s), 655(s).

Synthesis of $\{[Cd(L_3)_2]{\cdot}2DMF{\cdot}4H_2O\}_n$, (10). A mixture of $Cd(NO_3)_2{\cdot}6H_2O$ (0.50 mmol) and HL_3 (0.25 mmol) in DMF (3 ml) were placed in a Teflon-lined stainless steel autoclave and heated to 100 °C for 72 h. After the mixture was cooled to room temperature at the rate of 0.1 °C min^{-1}, colorless filtrate was put in open air. Block shaped crystals of **10** were collected within 2 h in 31% yield based on $Cd(NO_3)_2{\cdot}6H_2O$. Anal. calcd. for **10**: C, 50.72%; H, 5.01%; N, 10.43%. Found: C, 50.52%; H, 5.14%; N, 10.23%. IR (cm^{-1}): 3408(s), 3304(s), 3112(s), 3017(s), 2921(s), 2816(s), 2737(s), 1636(m), 1598(s), 1541(m), 1467(s), 1416(s), 1331(m), 1209(s), 1112(s), 1049(m), 1088(m), 973(s), 950(m), 902(s), 842(m), 847(m), 741(m), 688(s), 615(m).

X-Ray structural studies

Single crystal X-ray data were collected at 100 K on a Bruker SMART APEX CCD diffractometer using graphite-monochromated Mo-Kα radiation (λ = 0.71073 Å). Linear

Table 1 Crystal and structure refinement data for **1–10**

Compound	**1**	**2**	**3**	**4**	**5**	Compound	**6**	**7**	**8**	**9**	**10**
Formula	$C_{20}H_{14}N_4O_4Cd$	$C_{20}H_{14}N_4O_4Cu$	$C_{22}H_{18}N_4O_9Cd_2$	$C_{40}H_{33}N_8O_{11}Cd_2$	$C_{12}H_{10}N_2O_4Cd$	Formula	$C_{50}H_{48}N_{10}O_{13}Cd_2$	$C_{20}H_{14}N_4O_4Zn$	$C_{40}H_{30}N_8O_9Cd_2$	$C_{64}H_{56}N_{12}O_{15}Cd_3$	$C_{34}H_{40}N_6O_{10}Cd$
Fw	486.76	437.90	707.22	1026.56	358.63	fw	1221.79	439.74	991.54	1570.44	805.13
T/K	100	100	100	100	100	T/K	100	100	100	100	100
System	Orthorhombic	Trigonal	Monoclinic	Triclinic	Monoclinic	system	Tetragonal	Orthorhombic	Monoclinic	Monoclinic	Monoclinic
Space group	Pnna	$R\bar{3}$	$P2_1/n$	P1	$C2/c$	Space group	P 4_3 2_1 2	Aba2	$P2_1/c$	$P2_1/c$	$C2/c$
a/Å	13.571(3)	23.494(5)	13.710(5)	9.147(5)	18.725(3)	a/Å	14.865(5)	25.391(4)	19.370(5)	11.063(4)	18.290(2)
b/Å	16.443(5)	23.494(5)	8.481(3)	9.219(2)	8.100(5)	b/Å	14.865(5)	19.896(5)	10.292(3)	18.938(5)	16.292(5)
c/Å	8.265(4)	10.003(3)	19.343(5)	14.604(3)	16.297(4)	c/Å	13.139(4)	7.556(4)	20.590(4)	29.918(2)	13.675(4)
α (°)	90.000	90.000	90.000	97.973(5)	90.000	α (°)	90.000	90.000	90.000	90.000	90.000
β (°)	90.000	90.000	101.405(5)	104.956(4)	103.873(5)	β (°)	90.000	90.000	114.102(5)	99.625(3)	120.330(4)
γ (°)	90.000	120.000	90.000	104.565(5)	90.000	γ (°)	90.000	90.000	90.000	90.000	90.000
U/Å^3	1844.3(11)	4782(2)	2204.7(13)	1123.9(7)	2399.7(16)	U/Å^3	2903.3(16)	3817 (2)	3746.9(16)	6180(3)	3517.2(15)
Z	4	9	4	1	8	Z	2	8	4	4	4
ρ_{calc}, g cm^{-3}	1.753	1.369	2.131	1.517	1.985	ρ_{calc}, g cm^{-3}	1.386	1.530	1.758	1.687	1.520
F(000)	968	2007	1384	513	1408	F(000)	1216	1792	1976	3148	1656
μ/mm^{-1}	1.220	1.059	1.995	1.010	1.831	μ/mm^{-1}	0.798	1.322	1.205	1.102	0.687
Refl. collected	22242	7426	11521	5904	6007	Refl. collected	15748	9903	19427	32768	9899
Independent refl.	1496	1748	3570	4391	1958	Independent refl.	2430	2936	6166	8650	3418
GOF	1.061	1.122	1.095	1.094	1.125	GOF	1.223	0.996	1122	1.038	1.086
Final R_{in} [$I > 2\sigma(I)$]	R_1 = 0.0328 wR_2 = 0.0767	R_1 = 0.0549 wR_2 = 0.1779	R_1 = 0.0314 wR_2 = 0.0770	R_1 = 0.0514 wR_2 = 0.1375	R_1 = 0.0303 wR_2 = 0.0821	Final R_{in} [$I > 2\sigma(I)$]	R_1 = 0.0692 wR_2 = 0.2208	R_1 = 0.0347 wR_2 = 0.0758	R_1 = 0.0364 wR_2 = 0.0902	R_1 = 0.0580 wR_2 = 0.1465	R_1 = 0.0346 wR_2 = 0.0831
R_{in} alldata, F2 refinement	R_1 = 0.0385 wR_2 = 0.0833	R_1 = 0.0763 wR_2 = 0.2118	R_1 = 0.0378 wR_2 = 0.0901	R_1 = 0.0570 wR_2 = 0.1462	R_1 = 0.0390 wR_2 = 0.1084	R_{in} alldata, F2 refinement	R_1 = 0.0751 wR_2 = 0.2269	R_1 = 0.0435 wR_2 = 0.0821	R_1 = 0.0422 wR_2 = 0.0942	R_1 = 0.0782 wR_2 = 0.1638	R_1 = 0.0392 wR_2 = 0.0931
Flack parameter	—	—	—	0.001(5)	—	Flack parameter	−0.03(10)	−0.018(14)	—	—	—

absorption coefficients, scattering factors for the atoms and the anomalous dispersion corrections were taken from International Tables for X-ray Crystallography. Data integration and reduction were processed with SAINT[25] software. An empirical absorption correction was applied to the collected reflections with SADABS[26] using XPREP.[27] The structure was solved by the direct method using SHELXTL[28] and refined on F^2 by full-matrix least-squares technique using the SHELXL-97 program package. The non-hydrogen atoms were refined anisotropically except OW2 in **6**. Hydrogen atoms attached to carbon atoms were positioned geometrically and treated as riding atoms using SHELXL default parameters, while hydrogen atoms of water molecules were located from difference Fourier maps and refined freely keeping the O–H bond distances constrained to ~0.85 Å with the DFIX command. However, one hydrogen of OW3 in **4**, both hydrogens of OW1 and OW2 in **6** and hydroxyl proton of one EtOH solvent molecule in **9** could not be located even in successive difference Fourier maps due to their distorted nature. Also, due to distorted nature of pyridine molecule in **6**, several DIFIX and DANG commands were used to fix it. The crystal and refinement data are collected in Table 1 while selective bond distances and angles are given in Table S1 (Supporting Information‡).[14]

Acknowledgements

We gratefully acknowledge the financial support received from the Department of Science and Technology, New Delhi, India and a SRF from the CSIR to A. A and P.L. ECS acknowledges the financial support from Spanish Government, (Grant CTQ2006/03949BQU and Ramon y Cajal fellowship).

References

1 (*a*) H. K Chae, D. Y. Siberio-Perez, J. Kim, Y. B. Go, M. Eddaoudi, A. J. Matzger, M. O'Keeffe and O. M. Yaghi, *Nature*, 2004, **427**, 523; (*b*) C. Janiak, *Dalton Trans.*, 2003, 2781; (*c*) L. J. Murray, M. Dinca and J. R. Long, *Chem. Soc. Rev.*, 2009, **38**, 1294; (*d*) M. C. Das and P. K. Bharadwaj, *J. Am. Chem. Soc.*, 2009, **131**, 10942; (*e*) J. J. Perry, IV, J. A. Perman and M. J. Zaworotko, *Chem. Soc. Rev.*, 2009, **38**, 1400.

2 (*a*) P. Lama, A. Aijaz, E. C. Sañudo and P. K. Bharadwaj, *Cryst. Growth Des.*, 2010, **10**, 283; (*b*) A. Aijaz, E. C. Sañudo and P. K. Bharadwaj, *Inorg. Chim. Acta*, 2009, **362**, 4246; (*c*) E. Coronado, J. R. Galan-Mascaros and C. Marti-Gastaldo, *J. Am. Chem. Soc.*, 2008, **130**, 14987; (*d*) J. T. Brockman, T. C. Stamatatos, W. Wernsdorfer, K. A. Abboud and G. Christou, *Inorg. Chem.*, 2007, **46**, 9160; (*e*) L. J. Murray, M. Dinca and J. R. Long, *Chem. Soc. Rev.*, 2009, **38**, 1294.

3 (*a*) L. Ma, C. Abney and W. Lin, *Chem. Soc. Rev.*, 2009, **38**, 1248; (*b*) J. Y. Lee, O. K. Farha, J. Roberts, K. A. Scheidt, S. B. T. Nguyen and J. T. Hupp, *Chem. Soc. Rev.*, 2009, **38**, 1450; (*c*) J. J. Vittal, *Coord. Chem. Rev.*, 2007, **251**, 1781.

4 (*a*) L. Zhang, Y.-Y. Qin, Z.-J. Li, Q.-P. Lin, J.-K. Cheng, J. Zhang and Y.-G. Yao, *Inorg. Chem.*, 2008, **47**, 8286; (*b*) H. Han, Y. Song, H. Hou, Y. Fan and Y. Zhu, *Dalton Trans.*, 2006, **16**, 1972; (*c*) L. Han, M. Hong, R. Wang, J. Luo, Z. Lin and D. Yuan, *Chem. Commun.*, 2003, **20**, 2580; (*d*) J. L. Atwood, L. J. Barbour and A. Jerga, *Angew. Chem., Int. Ed.*, 2004, **43**, 2948.

5 (*a*) Q. Li, W. Zhang, O. S. Miljanic, C.-H. Sue, Y.-L. Zhao, L. Liu, C. B. Knobler, J. F. Stoddart and O. M. Yaghi, *Science*, 2009, **325**, 855; (*b*) B. Chen, L. Wang, F. Zapata, G. Qian and E. B. Lobkovsky, *J. Am. Chem. Soc.*, 2008, **130**, 6718; (*c*) M. Sarkar and K. Biradha, *Cryst. Growth Des.*, 2007, **7**, 1318.

6 (*a*) S. K. Ghosh, J. Ribas and P. K. Bharadwaj, *Cryst. Eng. Commun.*, 2004, **6**, 250; (*b*) H. Chun, H. Jung and J. Seo, *Inorg. Chem.*, 2009, **48**, 2043; (*c*) M. Eddaoudi, J. Kim, N. Rosi, D. Vodak, J. Wachter, M. O'Keeffe and O. M. Yaghi, *Science*, 2002, **295**, 469.

7 (*a*) J.-R. Li, D. J. Timmons and H.-C. Zhou, *J. Am. Chem. Soc.*, 2009, **131**, 6368; (*b*) F. Luo, Y.-X. Che and J.-M. Zheng, *Cryst. Growth Des.*, 2009, **9**, 1066; (*c*) N. L. Rosi, J. Kim, M. Eddaoudi, B. Chen, M. O'Keeffe and O. M. Yaghi, *J. Am. Chem. Soc.*, 2005, **127**, 1504.

8 (*a*) S. Yang, X. Lin, A. Dailly, A. J. Blake, P. Hubberstey, N. R. Champness and M. Schröder, *Chem.–Eur. J.*, 2009, **15**, 4829; (*b*) D. Tanaka, S. Horike, S. Kitagawa, M. Ohba, M. Hasegawa, Y. Ozawa and K. Toriumi, *Chem. Commun.*, 2007, 3142; (*c*) D. N. Dybtsev, H. Chun and K. Kim, *Angew. Chem., Int. Ed.*, 2004, **43**, 5033.

9 (*a*) K. Uemura, Y. Kumamoto and S. Kitagawa, *Chem.–Eur. J.*, 2008, **14**, 9565; (*b*) C. A. Black and L. R. Hanton, *Cryst. Growth Des.*, 2007, **7**, 1868; (*c*) D. M. Shin, I. S. Lee, Y. K. Chung and M. S. Lah, *Inorg. Chem.*, 2003, **42**, 5459; (*d*) Z. S. Bai, S. S. Chen, Z. H. Zhang, M. S. Chen, G. X. Liu and W. Y. Sun, *Sci. China Chem.*, 2009, **52**, 459.

10 (*a*) X.-M. Chen and M.-L. Tong, *Acc. Chem. Res.*, 2007, **40**, 162; (*b*) L. Han, X. Bu, Q. Zhang and P. Feng, *Inorg. Chem.*, 2006, **45**, 5736; (*c*) X.-M. Zhang, *Coord. Chem. Rev.*, 2005, **249**, 1201.

11 (*a*) Y.-Q. Lan, S.-L. Li, Y.-G. Li, Z.-M. Su, K.-Z. Shao and X.-L. Wang, *CrystEngComm*, 2008, **10**, 1129; (*b*) H. Deng, Y.-C. Qiu, Y.-H. Li, Z.-H. Liu, R.-H. Zeng, M. Zeller and S. R. Batten, *Chem. Commun.*, 2008, 2239; (*c*) Y.-T. Wang, H.-H. Fan, H.-Z. Wang and X.-M. Chen, *Inorg. Chem.*, 2005, **44**, 4148.

12 A. Aijaz, E. Barea and P. K. Bharadwaj, *Cryst. Growth Des.*, 2009, **9**, 4480.

13 (*a*) J.-P. Zhang, Y.-Y. Lin, X.-C. Huang and X.-M. Chen, *Chem. Commun.*, 2005, 1258; (*b*) C.-Y. Chen, P.-Y. Cheng, H.-H. Wu and H. M. Lee, *Inorg. Chem.*, 2007, **46**, 5691.

14 See Supporting Information (ESI)‡.

15 (*a*) L. Lisnard, P. Mialane, A. Dolbecq, J. Marrot, J. M. Clemente-Juan, E. Coronado, B. Keita, P. de Oliveira, L. Nadjo and F. Secheresse, *Chem.–Eur. J.*, 2007, **13**, 3525; (*b*) X. Li, R. Cao, W. Bi, Y. Wang, Y. Wang, X. Li and Z. Guo, *Cryst. Growth Des.*, 2005, **5**, 1651; (*c*) X.-J. Li, X.-Y. Wang, S. Gao and R. Cao, *Inorg. Chem.*, 2006, **45**, 1508.

16 (*a*) S. Horike, S. Hasegawa, D. Tanaka, M. Higuchi and S. Kitagawa, *Chem.Comm.*, 2008, 4436; (*b*) D.-C. Zhong, W.-G. Lu, L. Jiang, X.-L. Feng and T.-B. Lu, *Cryst. Growth Des.*, 2010, **10**, 739.

17 A. L. Spek, *PLATON*, Version 1.62, University of Utrecht, 1999.

18 X.-D. Chen, X.-H. Zhao, M. Chen and M. Du, *Chem.-Eur. J.*, 2009, **15**, 11974.

19 (*a*) F. Dai, P. Cui, F. Ye and D. Sun, *Cryst. Growth Des.*, 2010, **10**, 1474; (*b*) L. H. Xie, S. X. Liu, B. Gao, C. D. Zhang, C. Y. Sun, D. H. Li and Z. M. Su, *Chem. Commun.*, 2005, 2402; (*c*) W. Chen, J.-Y. Wang, C. Chen, Q. Yue, H.-M. Yuan, J.-S. Chen and S.-N. Wang, *Inorg. Chem.*, 2003, **42**, 944.

20 (*a*) T. K. Maji, K. Uemura, H.-C. Chang, R. Matsuda and S. Kitagawa, *Angew. Chem., Int. Ed.*, 2004, **43**, 3269; (*b*) L. Wen, Z. Lu, J. Lin, Z. Tian, H. Zhu and Q. Meng, *Cryst. Growth Des.*, 2007, **7**, 93.

21 (*a*) W.-P. Wu, Y.-Y. Wang, Y.-P. Wu, J.-Q. Liu, X.-R. Zeng, Q.-Z. Shi and S.-M. Peng, *CrystEngComm*, 2007, **9**, 753; (*b*) H.-L. Gao, L. Yi, B. Zhao, X.-Q. Zhao, P. Cheng, D.-Z. Liao and S.-P. Yan, *Inorg. Chem.*, 2006, **45**, 5980.

22 (*a*) L. Carlucci, G. Ciani, D. M. Proserpio and F. Porta, *Angew. Chem., Int. Ed.*, 2003, **42**, 317; (*b*) S. R. Batten, *CrystEngComm*, 2001, **3**, 67; (*c*) L.-P. Zhang, J.-F. Ma, J. Yang, Y.-Y. Pang and J.-C. Ma, *Inorg. Chem.*, 2010, **49**, 1535.

23 (*a*) G. A. Farnum and R. L. LaDuca, *Cryst. Growth Des.*, 2010, **10**, 1897; (*b*) P.-K. Chen, Y. Qi, Y.-X. Che and J.-M. Zheng, *CrystEngComm*, 2010, **12**, 720; (*c*) D.-R. Xiao, Y.-G. Li, E.-B. Wang, L.-L. Fan, H.-Y. An, Z.-M. Su and L. Xu, *Inorg. Chem.*, 2007, **46**, 4158.

24 J. M. Fevig, D. J. Pinto, Q. Han, M. L. Quan, J. R. Pruitt, I. C. Jacobson, R. A. Galemmo, Jr., S. Wang, M. J. Orwat,

L. L. Bostrom, R. M. Knabb, P. C. Wong, P. Y. S. Lam and R. R. Wexler, *Bioorg. Med. Chem. Lett.*, 2001, **11**, 641.
25 *SAINT* + , 6.02ed.; Bruker AXS, Madison, WI, 1999.
26 G. M. Sheldrick, *SADABS, Empirical Absorption Correction Program*, University of Göttingen, Germany, 1997.
27 XPREP, 5.1 ed. Siemens Industrial Automation Inc., Madison, WI, 1995.
28 G. M. Sheldrick, *SHELXL-97, Program for the Refinement of Crystal Structures*, University of Göttingen, Göttingen, Germany, 1997.

